Mathematical Methods for Treatment Planning in Deep Regional Hyperthermia

Dennis Sullivan, *Member, IEEE*

Abstract—**Computer simulation for treatment planning in deep regional hyperthermia cancer therapy using the Sigma 60 applicator involves the optimization of several parameters. Because the programs to simulate such treatments are computationally intensive, it is impractical to rerun the programs for each new set of input parameters. Techniques are described which accelerate this process by separating the problem into responses by individual quadrants and by employing an impulse response to get multiple frequencies per run. The implementation of these techniques using the finite-difference time-domain (FDTD) method is described. The accuracy is tested against three-dimensional measurements made in a homogeneous phantom. The result is a method capable of planning an optimum treatment for deep regional hyperthermia.**

I. Introduction

In the field of radio frequency (RF) hyperthermia cancer therapy, perhaps the most difficult problem is the treatment of deep-seated tumors, e.g., prostate, bladder, or cervix cancers. Treatments of this sort are difficult because RF energy is rapidly absorbed by human tissue. Therefore, treatment of sites more than a few centimeters below the skin surface with a single applicator is not often effective. One alternative is the use of several applicators positioned around the patients in a configuration which will allow constructive interference of the RF patterns of the applicators, a concept usually referred to as an annular phased array [1]. One such device is the Sigma 60 applicator of the BSD-2000 hyperthermia system, manufactured by the BSD Medical Corporation. This device consists of eight dipole applicators evenly spaced around a 60 centimeter annulus. The dipoles are arranged in four groups of two, referred to as quadrants (Fig. 1). Each quadrant is powered by its own linear class A power amplifier. All quadrants are driven at the same frequency, but each can have a separate amplitude and phase. It is this ability to impress independent amplitude and phase settings on the different quadrants which gives the Sigma 60 the ability to "steer" the power to the tumor site.

The frequency range of the Sigma 60 is 60 to 120 MHz. This frequency range, plus the variability of the amplitudes and phases of the four quadrants, presents numerous degrees of freedom in selecting the treatment mode. Thus far, phase selection is made primarily by the "line-of-sight" distance from each quadrant to the tumor site, as determined by the treatment software of the BSD-2000. This is accomplished by moving an icon on the screen of the computer console while running the treatment program. Frequency and amplitude are usually chosen by rule of thumb guidelines and the intuition of the operator. The line-of-sight selection of phases is less than desirable because it does not account for variations in the speed of the electromagnetic (EM) energy as it passes through different tissues [2]. Intuition will probably not result in the best selection of frequency and amplitudes.

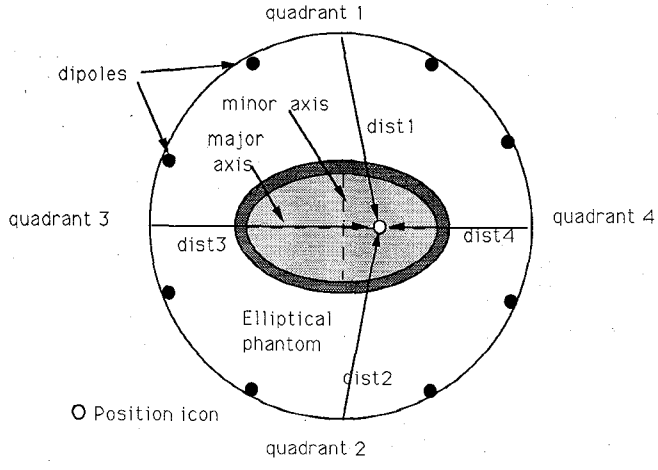

Fig. 1. Sigma 60 applicator containing an elliptical phantom.

It has long been recognized that computer simulation could play a role in treatment planning for annular phased arrays such as the Sigma 60 [3]–[5]. However, only recently have realistic three-dimensional models, capable of taking into account the full patient model, begun to appear [6]–[8]. The approach, thus far, has been the following: A model of the patient is constructed based on the EM properties of the various human tissues; a model of the Sigma 60 applicator is constructed around the patient model by using the EM properties of plastic, air, and metal. Then the treatment is simulated by assuming a sinusoidal $\boldsymbol{E}$ field from the dipoles of the Sigma 60. The phases and amplitudes of these sinusoids are set according to the phases and amplitudes being simulated. The

Manuscript received August 14, 1990; revised January 15, 1991. This work was supported by NCI Grants CA 40434 and CA 44664 and by grants for computer time from the Numerical Aerodynamic Simulation Program of the National Aeronautics and Space Administration and from the San Diego Supercomputer Center.

The author is with the Department of Radiation Oncology, Stanford University School of Medicine, Stanford, CA 94305.

IEEE Log Number 9143464.

solution of such a problem gives the specific absorption rate (SAR) distribution throughout the body for a given set of input parameters. What is really wanted is the input parameters necessary to give the most effective treatment. Even with state-of-the-art computer resources, when large detailed three-dimensional patient models are used, searching for the best treatments can entail enormous computer resources and operator time if it is necessary to rerun the program whenever one parameter is varied.

In this paper, two techniques are presented which utilize the finite-difference time-domain (FDTD) method to create a data base of information with which the operator can simulate a patient treatment interactively.

1) Superposition of E fields: Using one quadrant illumination, the FDTD program is run and the resulting complex $\boldsymbol{E}$ field is stored on a disk file for every point within the body being treated. When this has been repeated for all four quadrants, the data can be recalled, and the total $\boldsymbol{E}$ field for a given setting of amplitudes and phases on the four quadrants can be determined by the principle of superposition. The SAR can be determined from this $\boldsymbol{E}$ field.
2) Impulse response: Using an impulse response method, only one computer run is necessary to obtain the complex $\boldsymbol{E}$ fields for several frequencies in the range of interest.

We begin with a brief review of the FDTD method, followed by descriptions of the two techniques above. The accuracy of this method is then compared with measured data.

II. Description of the FDTD Method

The method used to calculate the EM fields within the Sigma 60 applicator is the FDTD method. This is a time-domain method which positions the $\boldsymbol{E}$ and $\boldsymbol{H}$ vectors around a unit cell, a concept first proposed by Yee [9]. The addition of radiation boundary conditions [10] and sinusoidal wave–source/observation conditions [11], [12] made this a computationally efficient means to calculate EM wave interactions with arbitrary structures. It has been used extensively to calculate scattering from metallic objects [12], [13]. Although it had seen some use in calculating EM energy absorption [14], it was only with the advent of supercomputers that detailed calculation of the EM absorption of a human body exposed to a microwave field has become possible, i.e., bodies modeled by 5000 cells or more [7], [15], [16].

The FDTD method is a straightforward implementation of the time-dependent Maxwell's equations:

$$\epsilon \frac{\delta \boldsymbol{E}}{\delta t} + \boldsymbol{J} = \nabla \times \boldsymbol{H} \qquad -\frac{\delta \boldsymbol{B}}{\delta t} = \nabla \times \boldsymbol{E}. \tag{1}$$

These vector equations can be written as six separate partial differential equations, one of which is

$$\frac{\partial E_z}{\partial t} = \frac{1}{\epsilon}\left(\frac{\partial H_y}{\partial x} - \frac{\partial H_x}{\partial y} - \sigma E_z\right). \tag{2}$$

This in turn, can be written as a difference equation for implementation on a computer:

$$\begin{aligned} EZ(I,J,K) &= CAZ(I,J,K)*EZ(I,J,K) \\ &\quad + CBZ(I,J,K)*[HY(I,J,K) - HY(I-1,J,K) \\ &\quad + HX(I,J-1,K) - HX(I,J,K)] \end{aligned} \tag{3}$$

where I,J,K represent position in the x, y and z directions, and EZ, HX, and HY represent the E_z, H_x, and H_y fields. CAZ and CBZ are parameters determined by frequency and cell size and by the electromagnetic characteristics of the material at point I,J,K. It is this ability to specify these parameters at every cell in the problem space which gives the method the ability to specify inhomogeneity, such as organs in the human body, to within the resolution of the cell size. Five similar equations are needed for the full representation of Maxwell's equations. It is assumed that the $\boldsymbol{E}$ and $\boldsymbol{H}$ vectors are positioned around a unit cell and that the collection of these cells form the three-dimensional lattice that contains the problem being simulated. All the simulations reported in this paper used a cell size of 1 cm. (Details of the method are well documented and will not be repeated here [6], [11], [12], [15].) The FDTD method has been shown to be extremely accurate in computing SAR's in biological bodies for both plane waves [15] and near-field applicators [7]. The method is particularly suitable for processing on a supercomputer, because the difference equations take full advantage of the vectorizing capability.

The model to simulate patient treatments in the Sigma 60 resides in a problem space of $74\times74\times68$ 1 cm cells. This requires ten megawords of core memory and about 200 CPU seconds on a Cray YMP supercomputer.

III. Superposition of E_z Fields

The near field of any antenna, such as the dipoles of the Sigma 60 applicator, is a complex pattern of $\boldsymbol{E}$ fields. In the case of the Sigma 60 dipoles, this means it has components in the direction tangential to and normal to the direction of the dipole (Fig. 2). However, it is only the component in the direction of the dipole, referred to as the E_z field in Fig. 2, which we are attempting to control by shifting the amplitudes and phases of the four quadrants. Since there are four separate sources, the four quadrants, the E_z field at any point (x,y,z) may be thought of as the superposition of the E_z field which would result if only one quadrant were activated, i.e.,

$$\begin{aligned} \overline{E}_{z\,\mathrm{Total}}(x,y,z) &= \overline{E}_{1z}(x,y,x) + \overline{E}_{2z}(x,y,x) \\ &\quad + \overline{E}_{3z}(x,y,x) + \overline{E}_{4z}(x,y,x) \end{aligned} \tag{4}$$

where $\overline{E}_{iz}(x,y,z)$ is the E_z field measured at point x,y,z with only the ith quadrant activated.

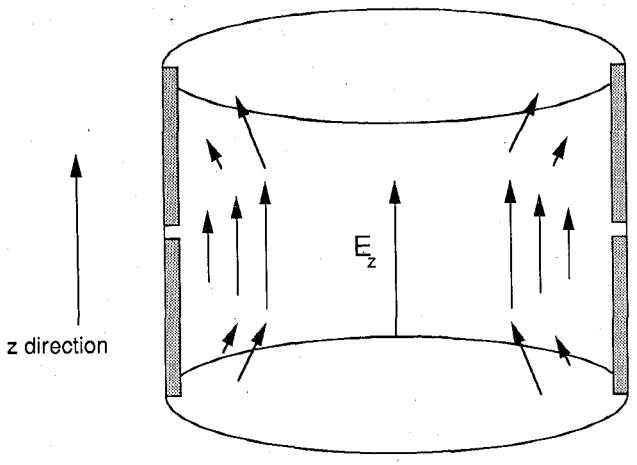

Fig. 2. The near field of the dipoles in the Sigma 60 applicator.

Now, suppose that only quadrant 1 is activated with an amplitude of 1 and no phase shift and that at a point within the treatment area x, y, z the amplitude and phase of the E_z field are measured as

$$\bar{E}_{z1}(x,y,z) = |E_{z1}| \cdot \angle \phi_1. \tag{5}$$

Then the E_z field which would be measured at the same point for an amplitude of α and a phase shift of ϕ_α on quadrant 1 would be

$$\bar{E}_{z1}(x,y,z) \cdot \alpha e^{j\phi_1+\phi_\alpha} = \alpha \cdot |E_{z1}| \cdot \angle \phi_1 + \phi_\alpha. \tag{6}$$

Therefore, if the four quadrants are given the following amplitude and phase settings:

$$\begin{aligned} &\text{quad 1:} \quad \alpha \angle \phi_\alpha \\ &\text{quad 2:} \quad \beta \angle \phi_\beta \\ &\text{quad 3:} \quad \gamma \angle \phi_\gamma \\ &\text{quad 4:} \quad \delta \angle \phi_\delta \end{aligned}$$

then the value of E_z at x, y, z is

$$\begin{aligned} \bar{E}_{z\,\mathrm{Total}}(x,y,z) = {} & \bar{E}_{z1}(x,y,z) \cdot \alpha e^{j(\phi_1+\phi_\alpha)} \\ & + \bar{E}_{z2}(x,y,z) \cdot \beta e^{j(\phi_2+\phi_\beta)} \\ & + \bar{E}_{z3}(x,y,z) \cdot \gamma e^{j(\phi_3+\phi_\gamma)} \\ & + \bar{E}_{z4}(x,y,z) \cdot \delta e^{j(\phi_4+\phi_\delta)} \end{aligned} \tag{7}$$

or, if we are only interested in the power deposition at a point, then

$$\begin{aligned} & 1/2 \cdot E^2_{z\,\mathrm{Total}}(x,y,z) \\ & \quad = 1/2\left[\alpha^2 \cdot E^2_{z1} + \beta^2 \cdot E^2_{z2} + \gamma^2 \cdot E^2_{z3} + \delta^2 \cdot E^2_{z4}\right] \\ & \qquad + |\alpha \cdot E_{z1}| \cdot |\beta \cdot E_{z2}| \cos\left((\phi_1+\phi_\alpha) - (\phi_2+\phi_\beta)\right) \\ & \qquad + |\alpha \cdot E_{z1}| \cdot |\gamma \cdot E_{z3}| \cos\left((\phi_1+\phi_\alpha) - (\phi_3+\phi_\gamma)\right) \\ & \qquad + |\alpha \cdot E_{z1}| \cdot |\delta \cdot E_{z4}| \cos\left((\phi_1+\phi_\alpha) - (\phi_3+\phi_\gamma)\right) \\ & \qquad + |\beta \cdot E_{z2}| \cdot |\gamma \cdot E_{z3}| \cos\left((\phi_2+\phi_\beta) - (\phi_3+\phi_\gamma)\right) \\ & \qquad + |\beta \cdot E_{z2}| \cdot |\delta \cdot E_{z4}| \cos\left((\phi_2+\phi_\beta) - (\phi_4+\phi_\delta)\right) \\ & \qquad + |\gamma \cdot E_{z3}| \cdot |\delta \cdot E_{z4}| \cos\left((\phi_3+\phi_\gamma) - (\phi_4+\phi_\delta)\right) \end{aligned} \tag{8}$$

from which the SAR may be determined by

$$\mathrm{SAR} = \sigma(x,y,z) \cdot E^2_{z\,\mathrm{Total}}(x,y,z). \tag{9}$$

Equation (8) may look formidable, but it is a single scalar equation. Therefore, if the complex E_z values for the four quadrants have been calculated and stored, the SAR at every point within the body for a new group of amplitude and phase settings can be calculated by (8), a process that takes only seconds, even on a minicomputer or workstation. (Note: Even though only the E_z fields are used to calculate (8), the FDTD program used to run the calculation for each quadrant is an implementation of the vector Maxwell equations, and calculates all three fields. It is only E_z which is saved and stored.)

IV. Impulse Response

In implementing the FDTD method, the source is usually specified as a sinusoid. This can be a plane wave coming from infinity [11], [12], [16] or the aperture in an applicator [6]. In the case of the Sigma 60, it is the gaps of the dipoles [6], [7]. What is wanted is the steady-state $\boldsymbol{E}$ or $\boldsymbol{H}$ fields. This is usually done by monitoring peak values until steady state is reached, normally after three to six time periods of the incident wave when dealing with biological problems. These peak values are used to determine field strength or SAR. This is described in detail in [11], [12], and [16].

As mentioned previously, the Sigma 60 works in the frequency range of 60–120 MHz. Let us say that we are interested in the SAR patterns at 70, 80, 90, 100, and 110 MHz. (High reflected power impedes use at 60 and 120 MHz, and intervals of less than 10 MHz are unnecessary.) To utilize the method of superposition described above, one run using each of the four quadrants at each of the five frequencies of interest would be necessary to build up the data base to be able to determine the SAR pattern for any possible treatment configuration, a total of 20 runs.

In general, when information is needed over a range of frequencies, there are various methods to illuminate the body with a more complex waveform than the single frequency sinusoid, and then extract the phase and amplitude information by Fourier analysis using a fast Fourier transform (FFT) [17]–[19]. For this application, there are two substantial drawbacks: One is that it is usually necessary to store the time-domain data over a substantial period of time for analysis when the FDTD program is completed. Such a technique is suitable when the problem only requires responses at a few select points throughout the problem space. But the application at hand is to determine the SAR throughout an entire body, typically 15 000–25 000 points. Storage of this much data, even temporarily, would be a logistical nightmare. The second drawback is that the FFT takes advantage of the structuring of the Fourier transform algorithm to bring the necessary computation down to a manageable amount.

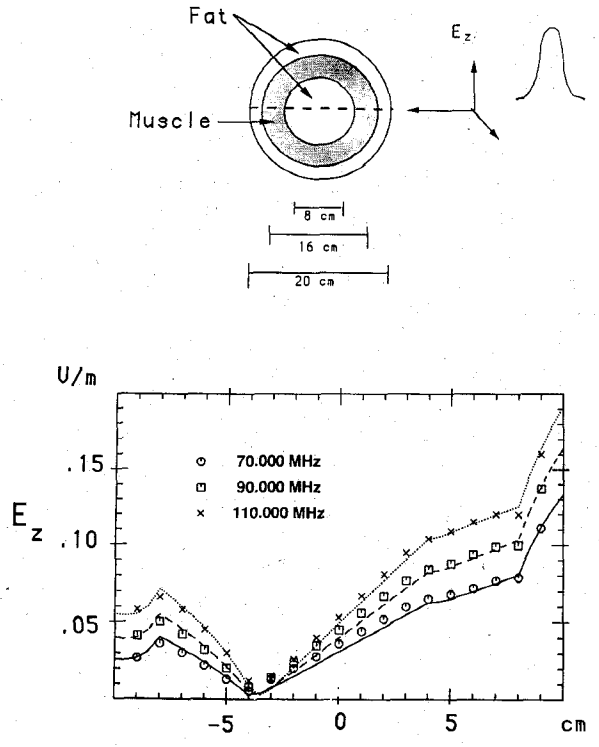

Fig. 3. Comparison between E_z fields as calculated by the FDTD impulse response method (symbols) and by the Bessel function expansion method (lines) for a fat/muscle/fat layered sphere.

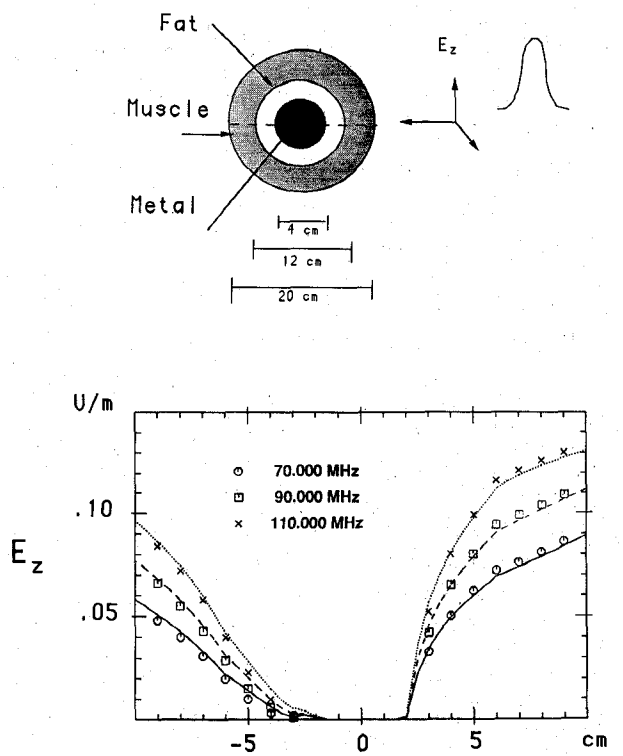

Fig. 4. Comparison between E_z fields as calculated by the FDTD impulse response method (symbols) and by the Bessel function expansion method (lines) for a muscle/fat/metal layered sphere.

However, this structuring also places limitations on the frequencies to be used. The frequencies are at intervals specified by the time interval and total time period. To ensure that all frequencies of interest are included in the output, extremely large numbers of data points would be necessary.

The following impulse response technique circumvents both of these obstacles. The Fourier transform is given by

$$EZ(f) = \int_{-\infty}^{\infty} ez(t) \cdot e^{j2\pi ft}\, dt. \tag{10}$$

If we write this as a discrete transform and assume that the function $ez(t)$ is causal,

$$EZ(f) = \sum_{n=0}^{N} ez(n \cdot \Delta t) \cdot e^{j2\pi fn\Delta t} \tag{11}$$

where Δt is the time interval between steps, and N is the maximum number of time steps needed to specify $ez(n \cdot \Delta t)$.

Equation (11) can be implemented by the following two lines of computer code added to the FDTD program:

$$\text{realpt}(i,j,k) = \text{realpt}(i,j,k) + ez(i,j,k) \cdot \cos(2\pi \cdot f \cdot n\,\Delta t) \tag{12a}$$

$$\text{imgpt}(i,j,k) = \text{imgpt}(i,j,k) + ez(i,j,k) \cdot \sin(2\pi \cdot f \cdot n\,\Delta t) \tag{12b}$$

where "realpt" and "imgpt" are the real and imaginary parts of the Fourier transform in (11), and i, j, and k represent the x, y, and z coordinates in the problem space.

Of course, two such equations are needed for each frequency. And in fact the overhead of this method versus the single-frequency FDTD technique is just two real matrices per frequency; the additional computational time for equations (12) is negligible. However, the peak detector algorithm also has a time and memory overhead, which has been eliminated. So requirements are about the same. This technique, along with a more detailed discussion of single frequency versus impulse response and the relative requirements, has been described by Furse *et al.* [20] as it applies to the calculation of radar cross sections.

In the past, the accuracy of the FDTD method has been tested by comparisons with the calculation of SAR distribution in layered dielectric spheres by Bessel function expansions [15]. Here we give only two additional examples to demonstrate the accuracy of the impulse response version. The E_z value along the main axis, as calculated by the FDTD impulse response method for several frequencies, is compared with the Bessel function expansion in Figs. 3 and 4. Fig. 3 shows a three-layered dielectric sphere of fat and muscle. Fig. 4 shows a metal sphere coated by a layer of fat and a layer of muscle. The metal core does not correspond to a typical biological medium, but makes a more challenging problem to demonstrate the accuracy of this technique. These comparisons are graphed at only three frequencies for clarity. Comparisons at 80 and 100 MHz are equally good.

V. Treatment Planning

Using the ideas explained in the previous two sections, here is a summary of the procedure taken to search for the optimum treatment plan:

1) Using CT scans, a model of the patient is created by assigning the appropriate value of dielectric constant and conductivity to each 1 cm cell based on the tissue type [7], [21], [22].
2) Using one quadrant at a time, the impulse response version of the FDTD program is run. The results, the complex values of E_z at every 1 cm cell within the body for each of the frequencies of interest (usually 70, 80, 90, 100, and 110 MHz), are stored on a disk file. This process is repeated for the other three quadrants.
3) A separate program uses the four data files containing the E_z values to determine the SAR distribution throughout the body via (8). The frequency, amplitudes, and phases (α's and ϕ's in (8)) are specified by the operator, and the SAR's are calculated and displayed. The display is color coded to represent SAR intensity and appears in 1 cm slices (corresponding to the CT scan used to create the input), one at a time, along the length of the body [22]. Since the calculation of the SAR's takes only seconds, this process may be quickly and easily repeated until the operator has found the best set of treatment parameters.

In step 3 above, the operator does not directly specify the phases but rather a focal point within the treatment area. This is used because the actual control software of the Sigma 60 specifies phases by moving an icon to a position on a grid (Fig. 1). The phase is then calculated from position by the equation

$$\phi_i = 0.1 \times (\text{frequency in MHz}) \times (\text{dist}_i - \text{dist}_{\max}) \quad (13)$$

where ϕ_i is the phase for quadrant i, dist_i is the distance from the given position to quadrant i in centimeters, and $\text{dist}_{\max}$ is the distance from the given position to the furthest quadrant in centimeters.

VI. Comparison with Experimental Results

In this section we present comparisons between SAR's measured in a phantom in the Sigma 60 applicator and the predicted SAR's from the methods described thus far. The phantom is an elliptical CDRH phantom with a major axis of 35 cm and a minor axis of 25 cm (Fig. 1). It has a 2 cm outer layer of material to simulate fat. It is filled with a material to simulate muscle having a relative dielectric constant of 70 and a conductivity of 0.68 S/m over the frequency range of interest (70–110 MHz) [23]. It has catheters at 2 cm intervals along the major and minor axes into which temperature probes can be placed for measurements (Fig. 1). Measurements are made by putting the phantom in the Sigma 60 and applying 1200 W of power while monitoring temperatures for several minutes. The rate of temperature rise is calculated to give an indication of SAR.

Fig. 5 shows a comparison at several frequencies for the case where equal amplitudes and phases have been applied to all four quadrants. Fig. 5(a) contains the SAR's predicted by the FDTD method; they are given as points connected by solid lines. (Calculated values have been multiplied by a normalization factor for easy comparison with measured data.) Fig. 5(b) contains the measured points given as circles connected by dashed lines. The SAR's along both major and minor axes are given. The four different lines in each plot, going from top to bottom, represent the data at the center transverse axis and at 5 cm, 10 cm, and 15 cm from the center transverse axis, respectively. The data are given in degrees centigrade per minute, the rate of temperature rise. Comparison between measured and calculated data is generally good, with some discrepancies at the higher frequencies. At 100 and 110 MHz, the measured data show sharply upturned edges along the minor axes but not the major axes; the opposite is true for the calculated. The exact reason for these discrepancies is unknown, but one likely cause is the cross-talk between the applicators.

Leybovich *et al.* [24] have suggested that the cross-talk between quadrants can play a significant role in the resulting SAR patterns. They have documented this by measuring the S (scattering) parameters among the four quadrants. Similar measurements have been made on the test setup described above using an HP 8753C network analyzer. Fig. 6 shows the $S34$ parameter, i.e., the cross-talk between quadrants 3 and 4. Note that at the higher frequencies, the magnitude is 0.3 to 0.35, a very substantial amount.

Because the S parameters can be accurately and rapidly measured, it would not be difficult to integrate their effect into the model, except for one thing: the exact phase is not known. Access to the dipoles of the four quadrants is through connectors on the side of the Sigma 60. From each connector there is a 229 cm cable running to a T connector from which two 13 cm cables run to the dipoles. The 229 cm cable is wound within the Sigma 60 to form an inductive loading [25]. This complex network between the connector port of the Sigma 60 and the actual dipoles makes it difficult to determine the phase at the dipoles. The phase displayed in Fig. 6 shows the relative phases among frequencies, but it also includes the phase shift from the input port of the Sigma 60 to the dipole inputs. Unfortunately, there is no way of knowing this additional phase shift so that it could be subtracted out.

Wust *et al.* [26] have measured the current distribution on the dipoles of the Sigma 60 applicator and have noted a lack of symmetry at the higher frequencies. This, too, could contribute to the discrepancies at 100 and 110 MHz. It is hoped that phenomena such as the current distribution and the cross-talk can be incorporated in future modeling programs.

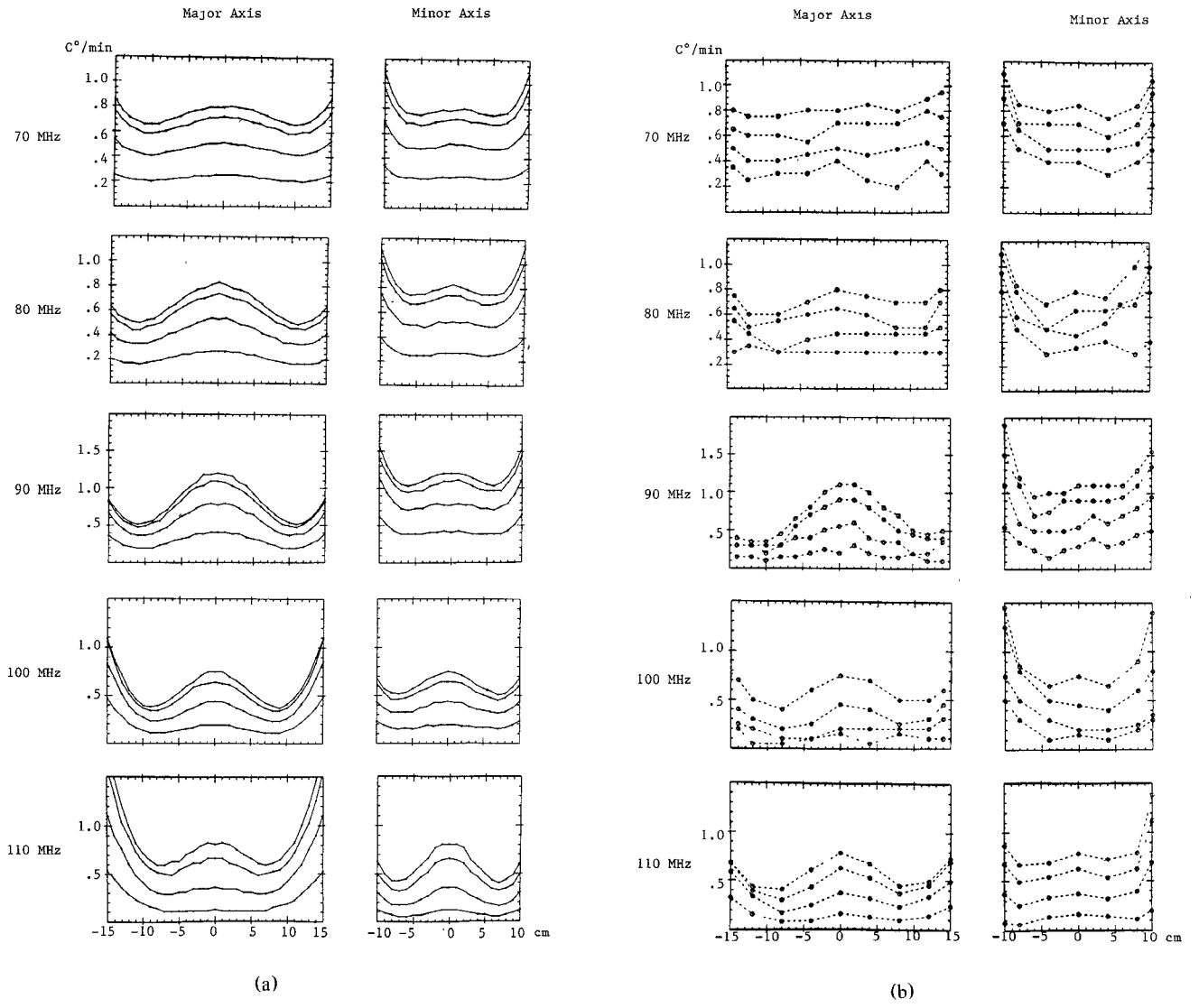

Fig. 5. (a) Simulated SAR distribution of an elliptical phantom in the Sigma 60 applicator with equal amplitudes and phases as calculated by FDTD method. The four lines in each graph represent, going from top to bottom, the data along the axes as calculated at the center transverse plane and at 5 cm, 10 cm, and 15 cm from the center transverse plane. (b) The SAR distribution measured in an elliptical phantom in the Sigma 60 applicator using a total of 1200 W of power for equal amplitudes and phases. The circles represent the measured points.

Fig. 7 shows comparisons along the major axis for various frequency, amplitude, and phase settings. (Remember, phase is specified by the position of the icon, which is indicated by the two digits in the brackets.) Agreement is quite good. It is worth noting that relatively small phase shifts in the focal point can produce substantial shifts in the pattern, which is borne out by both measured and calculated data. At 90 MHz, for instance, there is a substantial difference in patterns when the icon is at [0,0], [2,0], or [4,0].

One further comment: In using a homogeneous phantom to approximate human tissue, one would be likely to use values for the dielectric constant and conductivity of the order of about 2/3 muscle, in our case, a relative dielectric constant of about 50 and a conductivity of about 0.6 S/m. The phantom used in these measurements had a conductivity of 0.68, which is rather high. This is partly

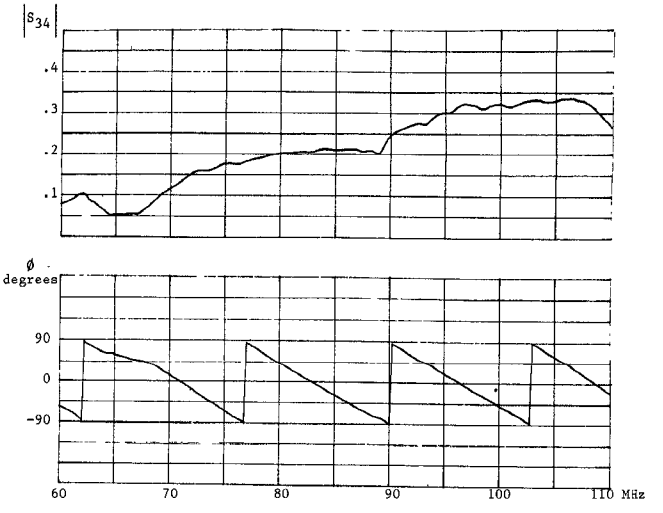

Fig. 6. Amplitude and phase of the S_{34} parameter as measured by an HP 8753C network analyzer.

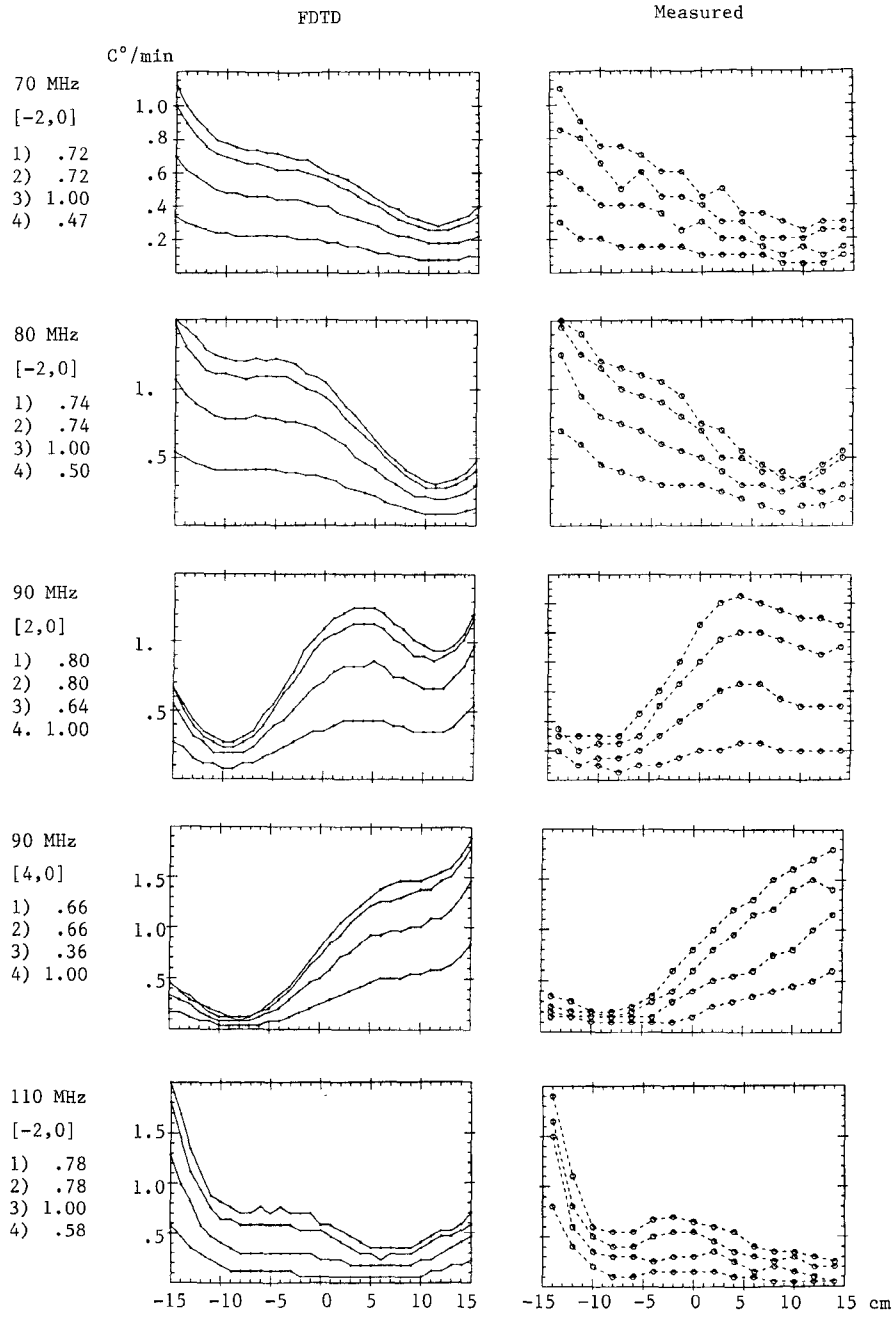

Fig. 7. Comparison of calculated (left) and measured (right) SAR data along the major axis of an elliptical phantom in the Sigma 60 applicator.

responsible for the large peaks along the minor axis in Fig. 5. A lower conductivity would give better central SAR's without such large peaks at the edges.

VII. Optimization

In that patient models typically consist of 15000 to 25000 points, a way is needed to quantify the output. In this discussion, we will use the following simple quantitative measure:

$$\text{SAR ratio} = \frac{\text{avg. SAR in the tumor}}{\text{avg. SAR in the body}}. \qquad (14)$$

For the purpose of demonstration, we have simulated an elliptical phantom in the Sigma 60 and arbitrarily designated a point 4 cm from the center along the major axis as a "tumor site" (approximately the position of the icon in Fig. 1). This "tumor" is about 2 cm in diameter and consists of seven 1 cm cells. Table I shows the SAR ratio which results as the focal point of the treatment planning software is moved along the major axis. Not surprisingly, the ratio reaches its maximum value when the focal point is over the tumor site. (This is usually not the case when dealing with actual patient models.)

By changing position and magnitudes of the quadrants and observing the effect on the ratio, it is not difficult for

TABLE 1
OUTPUT OF THE SAR OPTIMIZATION PROGRAM USING AN ELLIPTICAL PHANTOM WITH A TUMOR SIMULATED 4 CM RIGHT FROM CENTER ON THE MAJOR AXIS (NUMBER OF POINTS = 17205)

	Frequency	Icon Position	Amplitudes				SAR Ratio
1	90.0	[0.,0.]	10.00	10.00	10.00	10.00	1.359
2	90.0	[2.,0.]	7.60	7.60	5.30	10.00	1.728
3	90.0	[4.,0.]	6.60	6.60	3.60	10.00	1.905
4	90.0	[6.,0.]	6.00	6.00	2.70	10.00	1.896
5	90.0	[10.,0.]	5.30	5.30	1.80	10.00	1.431

the operator to find a good group of input parameters for a given frequency. However, in the future, it is hoped that the BSD-2000 will be made available with the ability to independently adjust the phases, instead of through icon position. This may present too many independent parameters to make a search by trial and error. It may prove helpful to use more systematic methods of optimization, such as a steepest descent algorithm. It will also be necessary to use a more elaborate weighting function than (14), for instance, one that penalizes SAR deposition to a vital organ or large SAR buildup on one side of the body. The important thing is that the problem has been quantified in such a way that mathematical techniques can be brought to bear.

VIII. DISCUSSION

In this paper we have described techniques to facilitate three-dimensional treatment planning for deep regional hyperthermia using the Sigma 60 applicator. Comparisons with measured phantom data have been presented. Two questions remain:

1) Is the use of only the dominant E_z field to calculate SAR justifiable?
2) Are the discrepancies between computed and measured data acceptable?

In any discussion dealing with accuracy one point must be remembered: We are dealing here with an optimization problem, i.e., given that we want to maximize energy deposition in a tumor site while minimizing it elsewhere, what are the input parameter settings which most nearly accomplish this? Therefore, any inaccuracy which is not great enough to cause a change in the estimate of the input parameters is not significant. First of all, these input parameters can only be specified within a certain accuracy using the treatment software of the BSD 2000. The power on the four quadrants is entered by adjusting four bar graphs on the screen of the computer terminal, making input somewhat qualitative. Given that there is also some discrepancy between specified and measured power, it is believed that amplitude can only be specified to 20%. The phases are adjusted by moving an icon on the screen which can only be specified to 1 cm accuracy in each direction, or 1.41 cm total, which is 10° at 90 MHz. Similarly, given some expected errors between measured and specified phase, it is believed that an error of about 20° could be expected at 90 MHz. Therefore, it may be said that inaccuracies in computing SAR that do not effect a change of 20% in amplitude or 20° in phase are not significant.

The influence of the normal $\boldsymbol{E}$ fields on SAR, the E_x and E_y fields in our discussion, manifests itself mainly at boundaries; it does not contribute much to SAR in the internal body. They do represent the majority of SAR energy at water/body interfaces distant from the middle transverse plane, especially the edge of the water bolus. Such fields often lead to patient discomfort, which can impede a treatment. However, such discomfort is not necessarily a linear function of SAR, so it is doubtful that including it would give the operator a meaningful prediction of discomfort. Besides, most such problems tend to be dealt with by the therapist as they occur, e.g., by adding another water bag between the patient and the main water bolus, which often eliminates an unwanted "hot spot" due to high SAR. Notice that the true SAR could be calculated merely by adding four more equations like (12a) and (12b) for each frequency, storing four more data files for the four quadrants, etc. It is not believed that the logistical overhead is worth it.

It has been shown that there are discrepancies between calculated and measured data, especially at higher frequencies. There is reason to believe that the cross-talk between quadrants and the asymmetry of the current distribution on the dipoles may be largely responsible, but a way to integrate these into the simulation has not been found. However, even at these higher frequencies the basic pattern is correctly predicted by the simulation, so that the best input parameters could still be found.

IX. CONCLUSION

It should be emphasized that the models described in this paper render *patient specific*, *three-dimensional* models. The comparisons in Section VI were made on a homogeneous phantom because this is the standard testing device for this field. But the techniques described in this paper are being used at this institution for true three-dimensional treatment planning in deep regional hyperthermia. A discussion of the way in which these methods are integrated into clinical use will be reserved for a later paper.

Lastly, the issue of computer resources necessary for the computations described in this paper must be ad-

dressed. Although generous supercomputer grants from government agencies make it possible for almost any researcher to use a supercomputer, it will be some time before computing power similar to that of the Cray YMP becomes available on a clinical basis. However, since only four runs of the FDTD program are needed per patient, these can be done on a computer with substantially less power, it will simply take longer to run.

Acknowledgment

The author is grateful to Dr. P. Turner of BSD Medical for many helpful discussions.

References

[1] P. F. Turner, "Regional hyperthermia with an annular phased array," *IEEE Trans. Biomed. Eng.*, vol. BME-31, pp. 106–114, 1984.

[2] P. F. Turner, "Hyperthermia and inhomogeneous tissue effects using an annular phased array," *IEEE Trans. Microwave Theory Tech.*, vol. MTT-32, pp. 874–882, 1984.

[3] M. F. Iskander, P. F. Turner, J. T. DuBow, and J. Kao, "Two-dimensional technique to calculate the EM power deposition pattern in the human body," *J. Microwave Power*, vol. 17, no. 3, pp. 175–185, 1982.

[4] V. Sathiaseelan, M. F. Iskander, G. C. Howard, and N. M. Bleehen, "Theoretical analysis and clinical demonstration of the effect of power pattern control using the annular phased-array hyperthermia system," *IEEE Trans. Microwave Theory Tech.*, vol. MTT-34, pp. 514–519, 1986.

[5] P. F. Turner, T. N. Schaefermeyer, and A. M. Turmeh, "Numerical modeling and treatment planning for deep local phased arrays," in *Proc. 5th Int. Symp. Hyperthermic Oncology* (Kyoto, Japan), Aug. 1988.

[6] C. Wang, O. P. Gandhi, "Numerical simulation of annular phased arrays for anatomical based models using the FDTD method," *IEEE Trans. Microwave Theory Tech.*, vol. 37, pp. 118–126, 1989.

[7] D. Sullivan, "Three-dimensional computer simulation in deep regional hyperthermia using the finite-difference time-domain method," *IEEE Trans. Microwave Theory Tech.*, vol. 38, pp. 204–211, 1990.

[8] K. D. Paulsen *et al.*, "Electromagnetic power deposition calculations on 3-d conforming meshes," presented at 10th Annual Meeting North American Hyperthermia Group, Apr. 7–12, 1990, New Orleans, LA.

[9] K. S. Yee, "Numerical solution of initial boundary value problems involving Maxwell's equations in isotropic media," *IEEE Trans. Antennas Propagat.*, vol. AP-17, pp. 585–589, 1966.

[10] G. Mur, "Absorbing boundary conditions for the finite-difference approximation of the time-domain electromagnetic field equations," *IEEE Trans. Electromagn. Compat.*, vol. EMC-23, pp. 377–382, 1981.

[11] A. Taflove, "Application of the finite-difference time-domain method to sinusoidal steady-state electromagnetic penetration problems," *IEEE Trans. Electromagn. Compat.*, vol. EMC-22, pp. 191–202, 1980.

[12] K. Umashankar and A. Taflove, "A novel method to analyze electromagnetic scattering of complex objects," *IEEE Trans. Electromagn. Compat.*, vol. EMC-24, pp. 397–405, 1982.

[13] R. Holland, "Threde: a free-field EMP coupling and scattering code," *IEEE Trans. Electromagn. Compat.*, vol. NS-24, pp. 2416–2421, 1977.

[14] A. Taflove and M. E. Brodwin, "Computation of the electromagnetic fields and induced temperatures within a model of the microwave-irradiated human eye," *IEEE Trans. Microwave Theory Tech.*, vol. MTT-23, pp. 888–896, 1975.

[15] D. M. Sullivan, D. T. Borup, and O. P. Gandhi, "Use of the finite-difference time-domain method in calculating EM absorption in human tissues," *IEEE Trans. Biomed. Eng.*, vol. BME-34, pp. 148–156, 1987.

[16] D. M. Sullivan, O. P. Gandhi, and A. Taflove, "Use of the finite-difference time-domain method in calculating EM absorption in man models," *IEEE Trans. Biomed. Eng.*, vol. 35, pp. 179–185, 1988.

[17] X. Ahang, J. Fang, K. K. Mei, and Y. Liu, "Calculations of the dispersive characteristics of microstrips by the time-domain finite difference method," *IEEE Trans. Microwave Theory Tech.*, vol. 36, pp. 263–267, Feb. 1988.

[18] R. J. Spiegel, M. B. A. Fatmi, S. S. Stuchly, and M. A. Stuchly, "Comparison of the finite-difference time-domain SAR calculations with measurements in a heterogeneous model of man," *IEEE Trans. Biomed. Eng.*, vol. 36, pp. 849–855, 1989.

[19] C. L. Britt, "Solution of electromagnetic scattering problems using time domain techniques," *IEEE Trans. Antennas Propagat.*, vol. 37, pp. 1181–1192, Sept. 1989.

[20] C. M. Furse, S. P. Mathur, and O. P. Gandhi, "Improvements to the finite-difference time-domain method for calculating the radar cross section of a perfectly conducting target," *IEEE Trans. Microwave Theory Tech.*, vol. 38, pp. 919–927, July 1990.

[21] B. J. James, "Three-dimensional CT-based patient modeling for hyperthermia treatment planning," presented at 10th Annual Meeting North American Group, Apr. 7–12, 1990, New Orleans, LA.

[22] B. J. James and D. M. Sullivan, "Creation of three dimensional anatomical patient models for hyperthermia treatment simulation using the FDTD method," submitted to *IEEE Trans. Biomed. Eng.*

[23] G. Hartsgrove, A. Kraszewski, and A. Surowiec, "Simulated biological materials for electromagnetic radiation absorption studies," *Bioelectromagnetics*, vol. 8, pp. 29–36, 1987.

[24] L. B. Leybovich, R. J. Myerson, B. Emami, and W. L. Straube, "Evaluation of the Sigma-60 applicator for regional heating in terms of scattering parameters," presented at 9th Annual Meeting North American Hyperthermia Group, Mar. 1989, Seattle, WA.

[25] P. F. Turner, personal communication.

[26] P. Wust *et al.*, "Einflussfaktoren und stoereffekte bei der steuerung von leistungsverteilungen mit dm hyperthermie-ringsystem BSD-2000, II. Messtechnische analyze," *Strahlungtherapie Onkologie*, to be published.

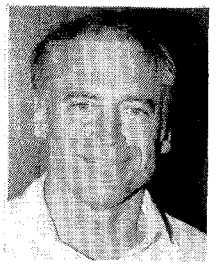

Dennis Sullivan (M'89) received the B.S. degree in electrical engineering from the University of Illinois in 1973. He then received the M.S. degree in electrical engineering in 1978, the M.S. degree in computer science in 1980, and the Ph.D degree in electrical engineering in 1987 from the University of Utah.

He is presently a research engineer in the Department of Radiation Oncology at the Stanford University School of Medicine, Stanford, CA. His interests are numerical modeling and drinking beer.